MOBIUS-STRIP-LIKE COLUMNAR FUNCTIONAL CONNECTIONS ARE REVEALED IN SOMATO-SENSORY RECEPTIVE FIELD CENTROIDS.

JJ Wright[1,2*], PD Bourke[3], OV Favorov[4].

[1] *Department of Psychological Medicine, Faculty of Medicine, The University of Auckland, Auckland, New Zealand.*

[2] *Liggins Institute, The University of Auckland, Auckland, New Zealand*

[3] *iVEC@UWA, University of Western Australia, Perth, WA, Australia*

[4] *Department of Biomedical Engineering, The University of North Carolina at Chapel Hill, Chapel Hill, North Carolina 27599-7575, USA*

***Correspondence:** *JJ Wright, Department of Psychological Medicine, Faculty of Medicine, The University of Auckland, Auckland, New Zealand.*
jj.w@xtra.co.nz

Keywords: cortical column, cortical development, synaptic organization, cortical response properties, neuromicrocircuitry, S1 segregates.

Abstract

Receptive fields of neurons in the forelimb region of areas 3b and 1 of primary somatosensory cortex, in cats and monkeys, were mapped using extracellular recordings obtained sequentially from nearly radial penetrations. Locations of the field centroids indicated the presence of a functional system, in which cortical homotypic representations of the limb surfaces are entwined in three-dimensional Mobius-strip-like patterns of synaptic connections.

Boundaries of somatosensory receptive field in nested groups irregularly overlie the centroid order, and are interpreted as arising from the superposition of learned connections upon the embryonic order.

Since the theory of embryonic synaptic self-organisation used to model these results was devised and earlier used to explain findings in primary visual cortex, the present findings suggest the theory may be of general application throughout cortex, and may reveal a modular functional synaptic system, which, only in some parts of the cortex, and in some species, is manifest as anatomical ordering into columns.

Introduction

The concept of the cortical column and its relation to response properties

It is widely acknowledged that Mountcastle's (Mountcastle 1955, 1997) concept of the cortical column was critical to subsequent development in the theory of the cerebral cortex (Hubel 1981; DeFelipe et al 2012). However, the concept has proved problematic (Purves et al 1992; Horton and Adams 2005). The terminology describing supposed variants and orderings into columns has become confused (Rakic 2008; DaCosta and Martin 2010). DeFilipe et al (2012) concluded that a comprehensive framework of the function and structure of columns has remained elusive, the classical criteria (shared response properties, shared input and common output) may need to be modified, and area-specific and species-specific variations more adequately defined, to achieve fundamental understanding of what columns are, and how they are used in cortical processes. Fundamental divergence of opinion was posed explicitly by Purves et al (1992) when they argued that "[columnar] patterns arise not because the functional organization of the brain demands them, but as an incidental consequence of the rules of synapse formation." This interpretation, forced to its limit, suggests that no functional modularity exists in the cortex, and therefore the task of its analysis is greatly

multiplied. However, there might exist modularity in the patterns of cortical synaptic connections, that become manifest as cellular anatomical order only under some circumstances. That is the position that will be argued here.

In this paper we apply a recent model for the organization of columnar structure in primary visual cortex (V1) to primary somatosensory cortex (S1) in areas anatomically not obviously columnar, to attempt to solve some of the dilemmas posed above. We will place emphasis on horizontal connectivity within cortex (Boucsein et al 2010) and on organised, modular, patterns of synaptic connections, rather than on spatial clustering of cell bodies into defined columns. To avoid the many terminological difficulties, we will simply define "macrocolumns" as variably resolved clusters of neurons sharing relatively dense short-range lateral connectivity, and distinguish separately the long-range horizontal patch connections, which also have clustered cell bodies, but have patchy areas of synaptic termination, patch-reciprocal and also terminating on the peripheries of macrocolumns. Reasonably clear macrocolumns in this sense are apparent only in V1 and in some other locales such as the barrel-based cortical columns representing vibrissae in S1 (Woolsey and Van Der Loos 1970) sensory systems in which the organisation of inputs is clear-cut, and this is only in some species and not in all situations with clear input demarcation (Purves et al., 1992).

Attempts to understand the relation between columnar organization and the response properties of single neurons have also struck problems (Swindale 1996; Blakemore and Cooper 1970; Blakemore and Van Sluyters 1975). In V1, visual line orientation has long been considered a primary property, but Fitzpatrick and colleagues (Basole et al 2003) have shown that orientation preference (OP) is a function not only of visual line orientation, but also of the angle of the line to the direction of motion, the speed of motion, and the length of the line. So long as stimulus properties are clearly defined, individual neurons show clearly tuned specific responses, whether or not response maps can be clearly resolved, as can be shown when OP tuning is contrasted in macaque and rat (Girman et al 1999). In V1, where response maps are relatively well resolved and continuous, Issa and colleagues (Issa et al 2008) have shown that the combination of cell responses to orientation, spatial frequency, temporal frequency and their bandwidth define the response maps. In S1, although macrocolumns are not clearly defined anatomically outside the cortical barrels, organisation of responses into combinations of stimulus features is also indicated by the way that receptive field (RF) boundaries form "segregates", as next discussed.

The finding of segregates in S1

Via dorsal column-medial lemniscus-cortical pathway, a homotypic representation of the skin surface is projected to the horizontal plane of the S1cortex (e.g, Marshall et al 1941) and in Mountcastle's conception of the columnar organization the homotypic map has depth from the pial surface to the white matter, with different afferent submodalities in a mosaic ordering. Exploring this concept in S1 forelimb representations, Favorov and colleagues (Favorov et al 1987; Favorov and Whitsel 1988ab; Favorov and Diamond 1990) advanced extracellular recording microelectrodes completely through the cortex at near-radial angles deviating on average about 22.5 degrees from the vertical. As expected, the more closely the path of descent approached the vertical (radial) track, the more similar became the RFs of the sequentially recorded single units. With the slight oblique drift of the electrode path they commonly encountered sequences of RFs that approximated an homotypic map, but there were also sudden discontinuities, where the RF of the next neuron found in the electrode's progress leapt to a relatively distant position on the skin surface – sometimes returning back closer to the prior localities as the electrode was still further advanced.

Using the skin locations of the maximum response (the "minRF") to tactile stimulation of local groups of neurons in a close vicinity to the tip of the recording electrode –rather than the full-extent RFs (maxRFs) of single neurons – Favorov and colleagues (Favorov et al 1987; Favorov and Diamond 1990) inferred the existence in S1 of functional macrocolumnar organization in a form of discrete,

300- 600μm wide columns, "segregates." In such a mosaic arrangement, a somatotopic map of minRFs is represented in a discontinuous fashion, with essentially unchanging minRFs within 300-600μm wide cortical zones and abrupt jumps of minRFs to new skin locations when crossing a sharp boundary separating any two such zones.

Favorov et al (1987) also found that when maxRFs, sequentially recorded along a near-radial penetration, were superimposed, they often shared a small area of common overlap. We will refer to these maxRF groups with common centre, forming nests of RFs, and indicating those neurons with spatial correlation of their inputs, as "nested RFs", "RF nests" or simply "nests". Such nests were related to segregates defined on the basis of minRF mapping: all the neurons sampled within the same segregate shared a common skin locus in their maxRFs and thus belonged to a single nest, whereas only about half on neurons sampled in a near-radial penetration across a segregate boundary shared a common skin point. Thus it appears that RF nests are centred on segregates but are larger than a single segregate.

We intend to show that the breaks in continuity of minRF positions found in S1 by Favorov and colleagues are explicable by a model of embryogenesis and synaptic self-organization independently developed to account for V1 columnar organization, and the nested RFs are an overlay of this primary order.

The Mobius model of macrocolumn embryogenesis, and its application to V1

During embryogenesis cells becoming cortical neurons divide and migrate to their mature positions while undergoing apotosis (Rakic 1998, 2009). Wright and Bourke (Wright and Bourke 2013) devised a theory for embryonic selection of neurons and their strongest synaptic connections that leads to a modular description of cortical organization – one in which the modular organization is that of the pattern of synaptic connections, but in which cellular order need be only variably apparent. The mechanisms of synaptic self-organization in this theory are similar to those argued in Purves et al (1992), with the argument further extended as follows:

In vitro, embryonic neurons fire synchronously and self-organize into "small worlds" (Downes et al. 2012) and secondly, synchronous firing of neurons prevents their apoptosis (Heck et al. 2008). We assume synchrony and cell survival are directly causally linked. Therefore the emergent cell network would be that selection of cell types, and their arrangement, maximizing the amplitude of synchrony for a given limit of total metabolic supply, as follows:

1. Simulations of electrocortical activity (Wright 2009, 2010) show minimization of the total axonal lengths of excitatory cells maximises synchrony, therefore maximizing uptake while minimizing metabolic cost/neuron.

2. In the dilute network of neuronal connections, metric distance of soma separation is proportional to "degree of separation" in the topological sense. Therefore minimizing axonal length selects a neural network with "ultra-small world" connectivity, implying the average density of synaptic connectivity declines with distance from each neuron's soma as a power function (Cohen and Havlin 2003).

3. A power function is the sum of exponential functions, and pre-synaptic densities of cortical neurons decline roughly exponentially (Braitenberg and Schuz 1991). Therefore ultra-small-world connectivity can be approximated by selection of subpopulations of neurons with suitable axonal ranges. In reality a considerable variety of excitatory cell types is encountered. For simplicity we treat these as only two ideal populations – a local type, with dense short-range horizontal connectivity, roughly corresponding to spiny stellate and pyramidal neurons with short axonal trees, and a type with long intracortical axons – the superficial patch cells. Cortico-

cortical connections are excluded from present consideration, but can be accommodated within the same theory. With only two subpopulations,

$$\rho(|\mathbf{q}-\mathbf{r}|^{-A}) \approx N_\alpha \lambda_\alpha e^{-\lambda_\alpha |\mathbf{q}-\mathbf{r}|} + N_\beta \lambda_\beta e^{-\lambda_\beta |\mathbf{q}-\mathbf{r}|} \tag{1}$$

ρ is the optimal pre-synaptic density/distance relation, $\mathbf{q}$,$\mathbf{r}$ are positions of excitatory cortical neurons, N_α and N_β are numbers of patch cells and local neurons respectively, and λ_α and λ_β are the corresponding inverse length constants of their axonal trees.

4. Any two populations of neurons conforming to eqn (1) sustain a magnitude of synchronous oscillation, J,

$$J \propto \int_{\mathbf{q}} \int_{\mathbf{r}} (N_\alpha \lambda_\alpha e^{-\lambda_\alpha |\mathbf{q}-\mathbf{r}|} + N_\beta \lambda_\beta e^{-\lambda_\beta |\mathbf{q}-\mathbf{r}|}) d\mathbf{q} d\mathbf{r} \tag{2}$$

5. Maximization of J then forces selection of cells in a ratio N_α / N_β according to differing axonal lengths of the given subpopulations. Two limiting cases arise.

At the limit where $\lambda_\alpha << \lambda_\beta$ eqn (1) requires $N_\beta >> N_\alpha$, and therefore maximization of J in eqn (2) requires cells with relatively short axons be closely situated, causing clustering into a macrocolumn. Consequently the cells with long-range axons must form connections at longer range, enforcing a "patchy" connection system. In the limiting case arrangement into a fully demarcated hexagonal periodic system must emerges, where

$$\frac{local\ cells}{local\ cells + patch\ cells} = \frac{N_\beta}{N_\alpha + N_\beta} \geq \frac{\pi}{2\sqrt{3}} \tag{3}$$

The relation in eqn. (3) is that of the most efficient packing, and follows from the ratio of area of a circle to a hexagon.

At an opposite limit, where $\lambda_\alpha \approx \lambda_\beta$ eqn (1) requires $N_\beta \approx N_\alpha$, and there is only one cell type. Cell bodies are intermingled, although eqns (1, 2) are still met, and the absence of a clearly columnar arrangement does not imply a loss of the small world organization. The left hand images in Figure 1 show these limiting cases, suggesting how varying species and cortical area macrocolumnar orders might arise as intermediates between the limiting cases.

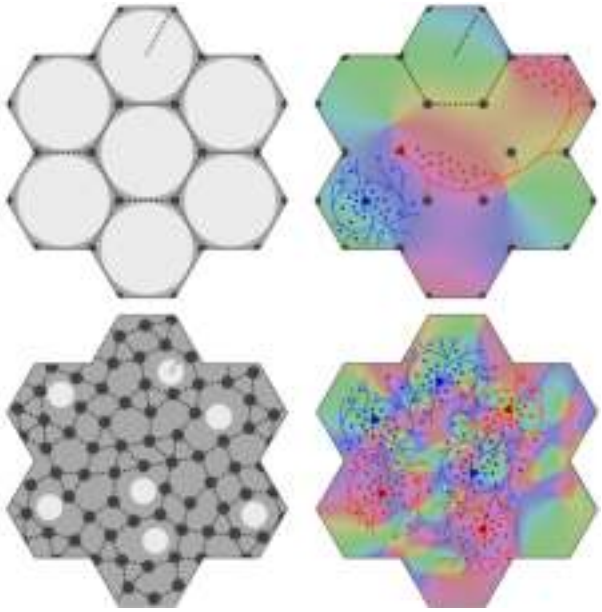

Figure 1. Variation of the structure of macrocolumns at limiting extremes of the axonal lengths and cell numbers in Figure 1. Top left: With large long/short axon length ratio, clearly resolved hexagonal organization emerges, with macrocolumns (white) surrounded by groups of patch cells (black dots). Top right: long (red line) patch connections link "like to like" OP (shown as background colour wheel) in contrast to highly clustered short intracortical axons (blue lines). Bottom left and right: near-complete loss of resolution when long/short axon ratio approaches 1.

6. Maximization of J also requires that the patch connections project a 1:1 map of activity in the surrounding cortex onto each macrocolumn. Competition between closely situated presynaptic terminals arising from the same cell but terminating on different cells, would force strong synaptic links to some neighbours and weak links to others. The requirement to form a 1:1 map can then be met only if the strong local connections within the macrocolumn form a closed network analogous to a Mobius strip, and the long-range patchy connections project the surrounding cortex onto this system as a Euclidean plane projected onto a Mobius strip. The right hand images in Figure 1 indicate how, in V1, this would force OP from 0-180 degrees to be arranged from 0-360 degrees about a singularity, and Figure 2 (top) shows how the strong and weak synaptic connections must be organised.

7. Interactions between local maps must also maximize J. Therefore patch connections must link "like to like" OP while forming multiple 1:1 maps, and adjacent macrocolumnar "maps" must be arranged so "like" map positions on adjacent macrocolumns are as closely situated as possible within the hexagonal frame, thus approximating a mirroring with continuity among adjacent maps. Figure 2 (bottom) shows these effects.

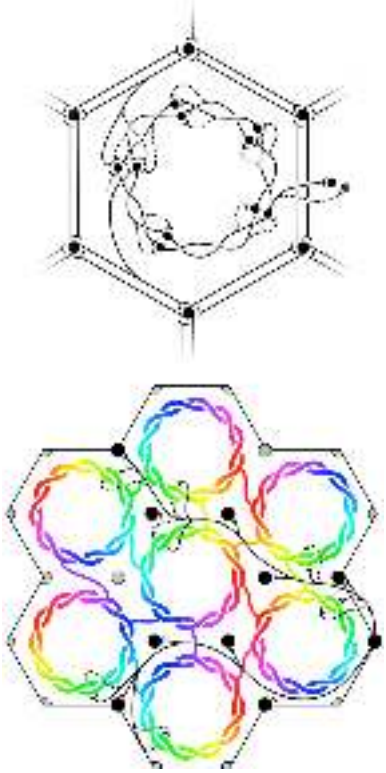

Figure 2. Maximization of synchrony with local synaptic competition leads to Mobius ordering, within macrocolumns.Top: Disposition of strong (solid) and weak (dashed) synapses in the developing neocortex. Bottom: "Like to like" patchy connections map the same part of the surrounding cortical field onto homologous cell positions on the Möbius configuration. Adjacent macrocolumns tend to mirror organization of OP.

Applied to V1 before eye-opening, this model is able to explain:

- The emergence of macrocolumns (in some species) in V1 and OP response maps, their singularities, and continuity at column margins (e.g. Bosking et al 1997).
- V1 approximation to hexagonal rotational periodicity (Paik and Ringach 2011; Muir et al 2011).
- Interspecies and inter-areal variation in superficial patch organization (Horton and Adams 2005; Muir et al 2011) and relative species invariance of intersingularity distances (Kaschube et al 2010; Keil et al 2012).
- Emergence (n some circumstances) of OD columns (Obermayer and Blasdel 1993).
- Emergence of superficial patch connections, "like to like" (Gilbert and Wiesel 1989; Muir et al 2011) with patch-sparing of macrocolumn centers (Sharma et al 1995; Muir and Douglas 2011).
- Variation of apparent OP with stimulus orientation, angle of movement relative to orientation, object velocity, and object length (Basole et al 2003).

and after eye-opening, consequent to visual stimuli and Hebbian learning:

- Later absence of cortical responses to stimuli of which the subject is deprived (Blakemore and Cooper 1970).

- The consolidation of learned cortical responses, producing selective tuning of cells stimulus orientation, spatial frequency, and temporal frequency (Issa et al 2008).

- Complex stimulus responses in higher visual areas.

The theory implies both the retention of pre-natal Mobius ordering into post-natal life (evidenced by reproduction of the results of Basole et al) and the overwriting of the earlier Mobius order by later learning, (accounting for the bandwidth tuning to classes of features shown in the work of Issa et al).

It is not proposed that variation of genetically prescribed cell types is the only source of variation of columnar order. Spatial and temporal resolution of signals in the input pathways, degree of approximation to "brown" cross-correlation in inputs, amount of convergence and divergence of axo-synaptic connections, and Turing pattern formation can all be expected to contribute to the apparent order, and might in principle be included in more developed forms of this model.

We turn now to the application of the model to S1, in areas where no clear anatomical macrocolumnar order has been shown.

Mathematical Considerations in application to S1

Viewed from above the V1 cortical surface, the Mobius-like arrangement of OP resembles a 2:1 map formed by squaring a complex vector, creating a local representation of global positions,

$$\pm P \rightarrow \frac{p^2}{|P|} \tag{4}$$

where P is a position in the visual field (and on the surface of V1), p is its mapped representation in the macrocolumn, the global and local maps have a common origin (P_0 and p_0) at the OP singularity, and are equivalently scaled.

However, this apparent 2:1 map conceals a 1:1 map in three dimensions, and application to sequential extracellular recordings on a trajectory passing from surface to depth in S1 requires consideration of three dimensions.

Applied in 3D, eqn. (1) and maximization of J in eqn. (2) requires local neurons with strong short-range synaptic connections to be packed closely together, forcing separation of the somata into two groups, one superficial and one deep, which we term "skeins" – the analog of each side of the paper in a paper Mobius strip. Onto these skeins of local cells projections conveyed by patch connections wind clockwise at one cortical level, and anti-clockwise at the other, with the projections circling a central zone, analogous to an OP singularity in V1.

Since complete skein separation could only be approached as ideal, at an intermediate level mixing and intertwining of the skeins is anticipated. The skeins are necessarily continuous at some angle directed from the central singularity, so mixing at the skeins would be lesser at the continuity. (See Figures 3, Top panels).

The interface between the skeins can be represented by a 3D representation of Mobius strip in Euclidean space, as is used in the top images of Figures 3a,b,c, and is given by:

$$\begin{aligned} x &= |p|\cos(\pm\vartheta + \varphi) \\ y &= |p|\sin(\pm\vartheta + \varphi) \\ z_M &= K|p|\sin((\pm\vartheta + \varphi)/2) \end{aligned} \tag{5a,b,c}$$

where x,y are Euclidean horizontal co-ordinates on the cortical surface, and z_M is the depth of the interface between the skeins. ϑ is polar angle, φ the angle of orientation of the macrocolumnar map versus the global coordinates; $(\vartheta+\varphi)\in[0,4\pi]$, and $\pm$ indicates chirality of the macrocolumnar map. K determines the stretching of the skein interface in cortical depth.

Interpenetration and entanglement of the upper and lower skeins is presumed at the intermediate zone of cortical depth, between $+z_M$ to $-z_M$, with greater separation of the skeins above and below.

The track followed by a recording electrode is:

$$z_D = ax + by + c \tag{6}$$

where z_D is the depth in the cortex reached by the probe, and a,b,c parameters of the track.

Thus, the positions at which maximum RF responses (subsequently treated as centroids of maxRFs) are discovered on the skin as the recording electrode advances follow a reverse mapping to that in eqn. (4) – viz:

$$\left|\sqrt{p}\right|\sqrt{p} \rightarrow \pm P \tag{7}$$

The sign $(\pm)$ in eqn. (7) is assigned positive if $z_D(x,y) > +z_M(x,y)$, negative if $z_D(x,y) < -z_M(x,y)$, and randomly assigned if $+z_M \geq z_D \geq -z_M$. That is to say, according to where the cell lies in relation to the skeins.

Specifying eqn. (7) for a pair of adjacent macrocolumns

$$\left|\sqrt{p-p_1}\right|\sqrt{p-p_1} \rightarrow \pm(P-P_1) \qquad \text{for } \mu_1(p)...\mu_{trans}(p) \tag{8a,b}$$

and

$$\left|\sqrt{p-p_2}\right|\sqrt{p-p_2} \rightarrow \mp(P-P_2) \qquad \text{for } \mu_{trans}(p)...\mu_n(p)$$

$\mu_1...\mu_{trans}$ and $\mu_{trans}...\mu_n$ are positions on the line of advance of the probe (eqn (6)), transiting between the adjacent macrocolumns, if the track does, at μ_{trans}. Positions p_1 and p_2 are the centres of the two maps, separated by a distance equal to the diameter of a macrocolumn. Adjacent macrocolumns each have representation via the patchy connections, of extensive areas of the skin, and overlap of the skin area represented considerable, and so to first approximation the skin area representations can be treated as identically centred, so that $P_1 \equiv P_2$.

The signs $\pm$ and $\mp$ in eqns (8a,b) carry the same meanings as in eqn (7) with the reversal $\pm$ to $\mp$ indicating the macrocolumns are so arranged that the entire Mobius mesh of one has opposite chirality to the other, forming mirror images, each of the other. For any pair of adjacent macrocolumns randomly selected, the axis of mirroring will be random relative to $\vartheta = 0$, but the patterns of RF centroids arising with variation of verticality of the recording electrode would be little affected. So, for simplicity, only mirroring along the $\vartheta = 0$ axis is considered in the next section.

Positions of sequential RFcentroids, predicted for electrode trajectories through S1

Figures 3,a,b,c, show expected results for the RFs sequentially discovered as an extracellular recording electrode passes through S1, from superficial to deep, through clockwise and anticlockwise skeins. Results vary depending on whether the electrode descends vertically, near-horizontally, or obliquely, and on whether the electrode remains within a single macrocolumn, or passes from one

macrocolumn into its neighbour.

In each of the three figures, the top frame shows the skein *interfaces* in a pair of macrocolumns, viewed obliquely from above the cortical surface. Colours on the colour wheel indicate the clockwise and anticlockwise winding of the skeins. The passage of the recording electrode is shown as a line of dots passing through the cortex, and thus penetrating the connection systems from top to bottom. Red dots represent positions in which the patch projections are winding clockwise, and blue dots positions in which the projections are winding anticlockwise.

The middle frames show the pair of macrocolumns and the electrode in horizontal plane view. Although the individual macrocolumns are shown as circular, we have assumed columnar continuity at their margins.

The bottom frame shows the positions of the centroids of RFs of the neurons found sequentially by the penetrating electrode. (Supplementary movies provided with this paper show the sequential development, as the electrode is advanced.) RF centroids associated with positive-valued solutions on the right-hand side in eqns (8a,b) are marked red, while negative-valued solutions are marked blue. In the intermediate region where the skeins may mix, RF centroids are randomly assigned red or blue.

In these images no allowance has been made for cortical anisotropy, nor recording noise, and the bottom images have been normalized in scale, and centered.

Figure 3a shows results typical of a near-vertical electrode penetration remaining within a single macrocolumn (a type I penetration). Sequential RF centroids as the electrode descends are tightly clustered until a “jump” occurs in the sequence, as the electrode passes from one skein to the other, and a second cluster of RF centroids begins and persists until the cortex is completely penetrated. If the electrode track is slightly off vertical, the RF centroids may be less tightly clustered, and progress in one direction until the jump occurs, and in the opposite direction after the jump. If the electrode track passes through the less demarcated zone between skeins sequential centroids may jump back and forth between the clusters.

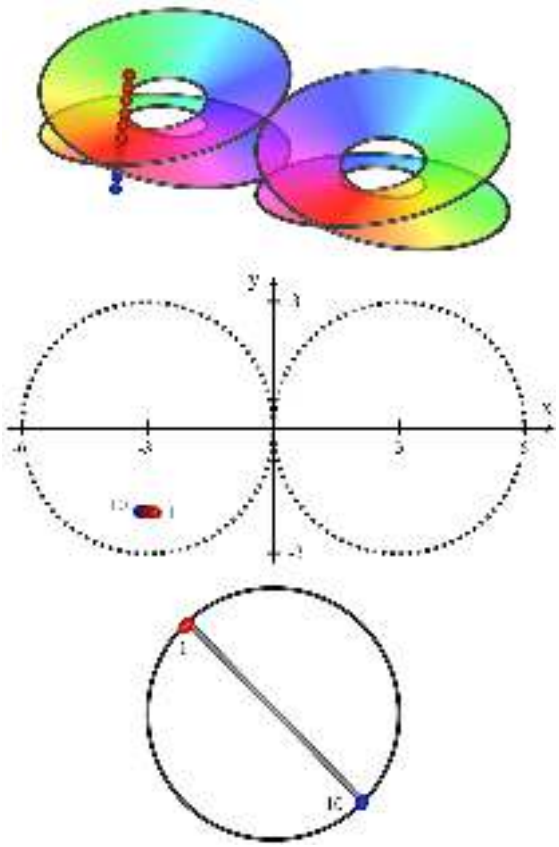

Figure 3a. Near-vertical passage of a recording electrode through S1, from (x,y,z)= (-2.8, -2, 2) to (-3.2, -2,-1.2), K=0.4.
Top: Interfaces demarcating synaptic skeins in two adjacent macrocolumns, viewed from obliquely above cortical surface. Each of the left and right pairs of disks represent the interfaces between an upper skein and a lower skein of local cells, receiving projections via patchy connections from surrounding cortex, with a mixed area between upper and lower disks. The projections wind clockwise in one skein, and anticlockwise in the other. Colours of the spectrum on the disks indicate the direction of winding, reversed in the pair of macrocolumns. The track of the recording electrode is marked with red and blue dots to distinguish neurons in clockwise and anticlockwise skeins.
Middle: positions of recorded neurons in plan view. First and last neurons discovered by the advancing recording electrode numbered accordingly.
Bottom: RFs centroids, strongly clustered into two groups, associated with clockwise and anticlockwise skeins respectively.

Figure 3b shows results typical of the passage of the recording electrode at an angle approaching the horizontal, remaining high enough in cortex to pass partly across the border of a pair of macrocolumns (a type II penetration), with only the upper skeins of both columns penetrated. In this case the sequential progression of RF centroids is in well-differentiated steps in one direction, then the reverse direction, as the junction between macrocolumns is crossed, encountering the mirror-image reversal of skeins in adjacent macrocolumns. Were the electrode to pass horizontally through deep cortex, a similar result (but with reversed positions of sequential RF centroids) would be obtained.

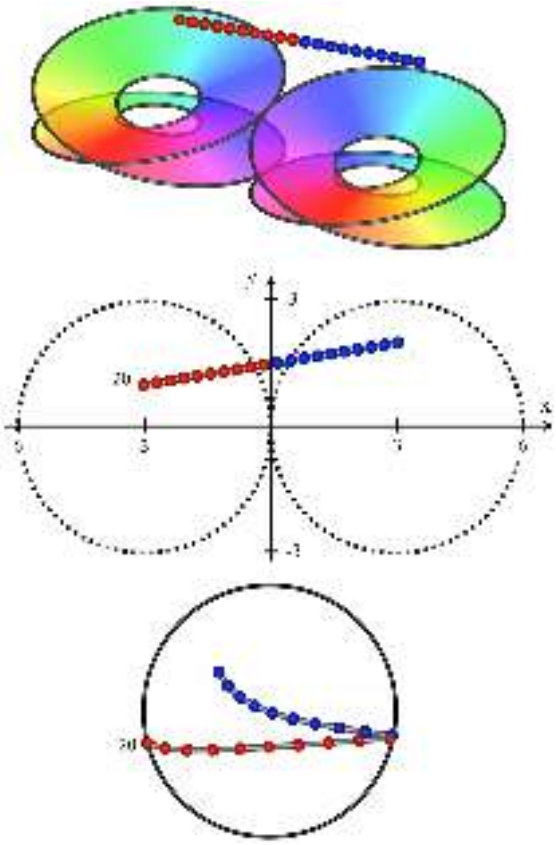

Figure 3b. High horizontal passage of a recording electrode, crossing the junction of two adjacent macrocolumns, from (x,y.z) = (3,2,2) to (-3,1, 2). RF centroids form columns of progressing sequentially in one direction, until the junction of the two macrocolumns is crossed, after which point the direction of sequential progression is reversed.

Figure 3c shows an intermediate result, also a type II penetration, where the electrode has passed obliquely through the system, encountering a substantial fraction of neurons lying in the poorly demarcated zones between skeins. A mixture of effects arises, all producing "jumps" backwards and forwards.

This continuum of outcomes permits model fitting to experimental data.

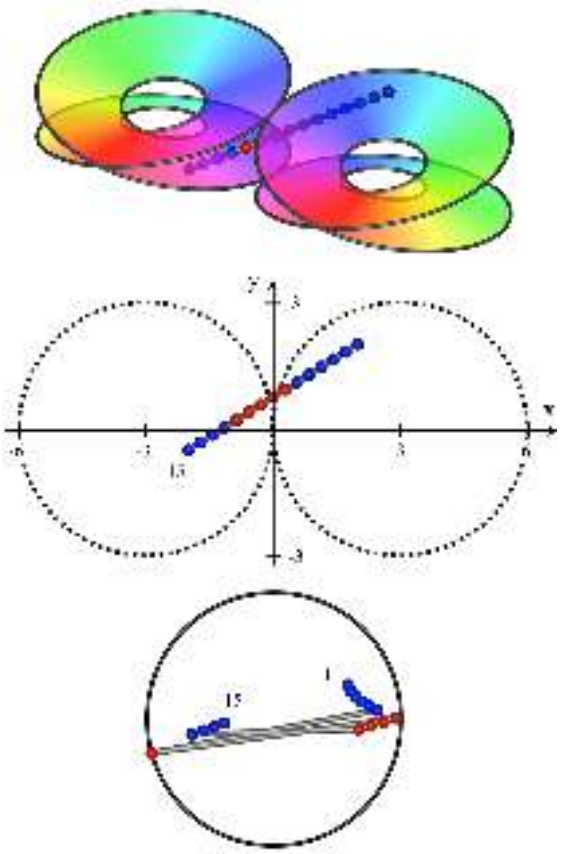

Figure 3c. Oblique passage of the electrode, from (x,y,z) = (2,2,1) to (-2,-0.5, -1). The path of penetration both crosses the junction of adjacent macrocolumns and passes through zones in which clockwise and anticlockwise skeins of synaptic connections are poorly demarcated. Centroids of RFs associated with clockwise and anticlockwise skeins are entangled, but sequential progression of RFs associated the clockwise skein is still in the reverse direction to those associated with the anticlockwise skein.

Methods

All data were obtained by digitising the original maxRF drawings of single neurons studied by Favorov, Whitsel and Diamond in 1980s at the University of North Carolina at Chapel Hill and published in Favorov et al (1987), Favorov and Whitsel (1988a) and Favorov and Diamond (1990).

Physiological RF recordings

Experimental methods are described for monkeys in Favorov and Whitsel (1988a) and for cats in Favorov and Diamond (1990).

A recording chamber was installed over a small opening in the skull over the S1 forelimb region of *Mucaca fascicularis* monkeys or domestic cats. Dura was removed under general anesthesia, surgical sites infiltrated with local anesthetic, then halothane anesthesia was discontinued, and the subjects were immobilized with gallamine triethiodide, placed on positive pressure ventilation, and EEG monitored.

Using electrolytically sharpened, glass-insulated tungsten electrodes in arrays, closely spaced radial penetrations each yielded extracellular records from 11-43 neurons. The effective sampling radius of the electrodes was estimated at <50 μm. Single units were isolated on the basis of the amplitude and the shape of the recorded action potentials; multi-unit recordings were excluded. For each isolated

single unit demonstrated to receive input from the skin, the modality (hair movement, skin contact, or movement over the skin) of the effective peripheral stimuli, and the rate of adaptation of the neuronal response to maintained adequate stimulation were determined. The stimulus that evoked the most vigorous response when applied to the most sensitive part of the RF was used to map RF boundaries. Cells responding primarily to deep tissue stimuli were excluded.

Maps of skin RF boundaries were transferred to a standard forelimb drawing and subsequently digitised for analysis. Electrolytic lesions were placed in selected penetrations to enable reconstruction of electrode tracks in the serial histological sections prepared for each brain.

Centroids of RFs were computed from their boundaries, and the centroids plotted on standard forelimb drawings. In a few instances divided RFs were found, that could not be defined within a single enclosing boundary, so in these cases the centroid was calculated for the overall RF.

Preliminary identification of RF centroid patterns before model fitting

In each dataset, progressions of the centroid positions in the order they were recorded were noted. Three typical classes of results were found, corresponding to those described by Figures 3a,b,c, with an overlay of spatial noise.

1. Cases in which there is one cluster of points, and a few outliers or a smaller cluster. For model fitting, centroids in the first cluster (in numerical order of the neurons recorded) were designated red, and those of the outliers/second cluster blue, in accord with colours ascribed in Figure 3a.

2. Cases in which there is a clear sequence of points going continuously in one direction, then reversing back in the other direction. The initial direction of progress of the centroid progress in order was designated red, the reverse progress blue, in accord with the colours ascribed in Figure 3b.

3. Cases in which the points in sequence "jump" back and forth irregularly, without distinct clusters. In accord with Figure 3c, points following a jump in one direction were designated red, jumps in the opposite direction blue.

Since these data were to be fitted to a theoretical model utilizing a maximum of two adjacent macrocolumns, the model can be fitted only to datasets in which there is a maximum of three distinct clusters or sequential runs of red and blue points in a single direction. More than three clusters or runs were apparent in some datasets obtained in a single electrode penetration. Then the dataset was split into sections each of which could be fitted to the model individually, and these subsets are subsequently referred to as "splits".

A few datasets were obtained in which the centroids progressed in jumps both proximal and distal as well as ulnar and radial preventing orderly numbering. These data were set aside, considered as artefactual or arising from situations outside the theoretical model to be used in fitting – e.g., they might arise from electrode penetration of cortical areas on junctions between three macrocolumns.

Calculations were then made to allow for effects of cortical anisotropy. Figure 4 shows a typical RF against a cat's forepaw outline. The size and elliptical shape of the RF reflects the anisotropic representation of the skin surface in S1 (e.g., Kaas et al 1979) in which cortical representation is of roughly inverse size to skin extension. Length of the longest axis of each RF and its angle to a reference frame on the animal's limb, and length on the broadest axis orthogonal to the long axis, were measured and averaged over the RFs in a dataset. Subsequently the average anisotropy for the dataset was applied to the spatial distribution of theoretical points at each trial of fit.

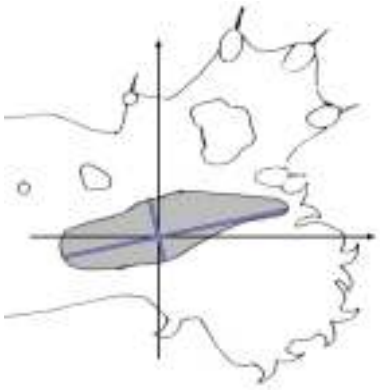

Figure 4. Calculation of cortical anisotropy for an RF. Against an outline of the cat's standard forelimb with reference axes, the blue lines indicate the longest and broadest axes of the RF.

Model fitting

Best fit of theoretical model to experimental data was found for each experimental dataset of n RF centroid positions, by: (a) Translating their centre-of-mass to the origin, and normalising the extension of the plot from the origin. (b) Computing sets of theoretical positions $P_1 ... P_n$ predicted for all possible probe tracks from $\mu_1 ... \mu_n$ equidistant neuron positions (eqns. (8a,b)), thus choosing at random over the full range of possibilities for parameters a, b and c, in eqn. (6). (c) Transforming each random theoretical RF centroid plot to eliminate the effects of cortical anisotropy, as described in the prior section, normalizing their scaling and translation as for the experimental data, and randomly rotating the plot (d) Calculating the sum of squared deviations of theoretical positions $P_1 ... P_n$ from their experimental equivalents in each trial and (e) Selecting the best fit.

For each dataset 120 Billion random matches were tried, and best-fit results plotted.

Relative goodness of fit of separate datasets was compared by RMS noise/signal ratio – that is, for each dataset, the square root of the sum of squared distances of each of the n theoretical and experimental pairs of centroids was divided by the sum of squared distances of the experimental centroids from the origin and results tabulated.

Construction of nested RFs

The RFs were superimposed and the number of RFs overlapping at each position on the standard forelimb counted, to obtain local maximum counts. Local maxima thus indicated nest centres, as those with the largest number of contributing RFs. We then superimposed upon each of the centres all those RFs within which that centre lay, thus obtaining all nested RFs for the dataset. Each nest was plotted on the standard forelimb outlines, and the colour spectrum from red to blue used to indicate their density of overlap.

Results

Datasets and exclusions

From the existing monkey data, we excluded experiments in which RF outlines were confined to fingers, as this distribution made calculation of RF centroids problematic. From cats we excluded datasets in which a large fraction (about 50%) of RFs were non-sequential, because interposed neurons had not had RF boundaries recorded but were used for a different purpose. We retained one dataset (CAT8615p1) that had only two neurons' recordings missing in sequence, and in that instance interpolated blank, unweighted positions during model fitting.

The only other exclusions were two monkey datasets in which the plot of centroids progressed in steps proximal and distal as well as radial and ulnar, preventing orderly numbering, and were therefore considered artefactual or obtained from an irregular cortical area.

This left 22 datasets, composed of either complete sequences passing through the cortex (10 datasets) and 12 "splits", divided as stated in Methods (6 complete sequences, each divided into 2 split datasets). The 22 datasets were obtained from 7 animals (3 cats and 4 monkeys, 7 datasets from cats and 15 from monkeys) providing RF outline data from 310 neurons.

Electrode track histology

Penetrations were never perfectly perpendicular to the cortical surface. A 200 μm advance of the electrode resulted in an average displacement of 50 μm in the horizontal plane. In comparing experimental data with the theoretical model, we have made no attempt to directly relate histological measurement of obliquity of the electrode track to the outcomes, because track variation was markedly overshadowed by the effect of part of the limb in which the measured RFs were clustered. If located distally in the limb, results approximated expectation for a vertical electrode passage. If in the proximal limb, the results approached expectation for oblique or almost horizontal electrode passages. That is, cortical anisotropy, by affecting relative size of cortical representation of equal skin areas, predominated in determining the apparent obliquity of the electrode track, because the larger the cortical representation the less the apparent lateral drift across the skin representation.

Representative results of model fitting

Figures 5a,b,c,d,e,f show representative results. Complete analyses of all datasets are supplementary to this paper, and are commented on further at the end of this section. An example from each of cat and monkey is shown, for each of the three types on the continuum of possibilities forecast in Figures 3a,b,c.

In the top left corner, each figure has the label given the data in the original experiments of Favorov and colleagues. Top left is the plot of RF centroids, and top right the plot is referred to the cat or monkey forelimb outline. Centroids are coloured red or blue according to the conventions described in Methods. Bottom left is the best-fit theoretical result, with, shown in green, the corresponding connected line through the experimental centroids. Bottom right, the two circles show the pair of theoretical macrocolumns and needle track in plane view.

The values shown in each figure as "RF anisotropy" give the average ratio of the long to the short axes of the RFs in a dataset, and the angle of the long axis to the reference axes. "Rotation" is the angle through which the theoretical best fit was rotated. It is, therefore, a measure of the orientation of the hypothetical local map.

RMS noise/signal ratios (goodness of fit) ranged from 0.23 to 1.06, the lower values tending to occur with more proximal RF datasets. Mean RMS noise/signal over all datasets was 0.62. Tabulated results are provided as Supplementary to this paper.

Where the allocation of centroids as red or blue was other than in accord with the protocol in Methods, inferior goodness of fit (higher RMS Noise/signal in each dataset) resulted.

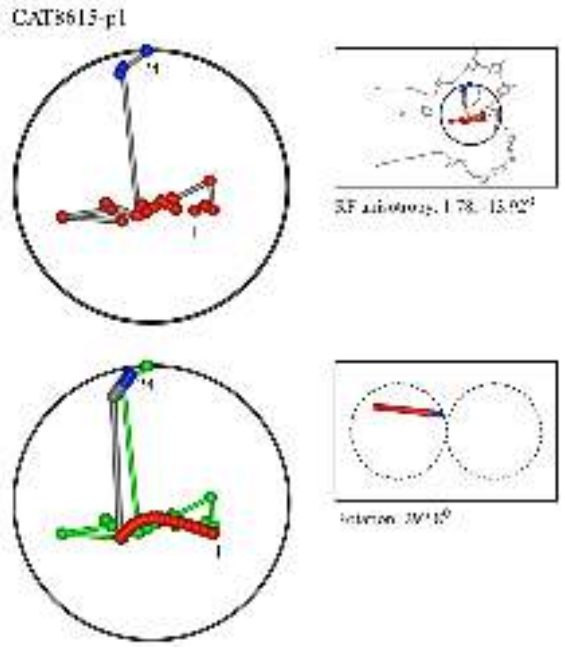

Figure 5a. A "vertical" penetration of cortex in a cat.
Layout of Figures 5a,b,c,d,e.f.
Top Left: Experimental data - centroids of RFs, red and blue colours indicate hypothetical position within Mobius organisation of macrocolumn. Top Right: RF centroids on cat forelimb outline. Bottom Left: Best fit of theoretical model to experimental data. Background green line is outline of experimental plot. Bottom Right: Theoretical construction of passage of recording electrode, on plane view of cortical surface.

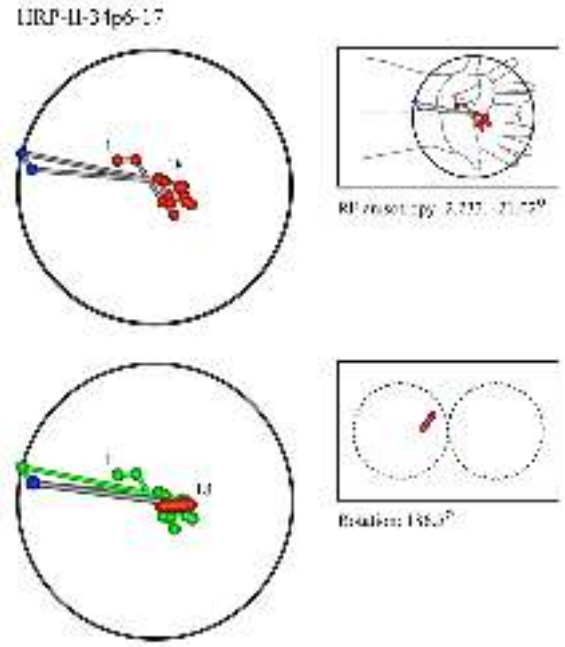

Figure 5b. A "vertical" penetration of cortex in a monkey.

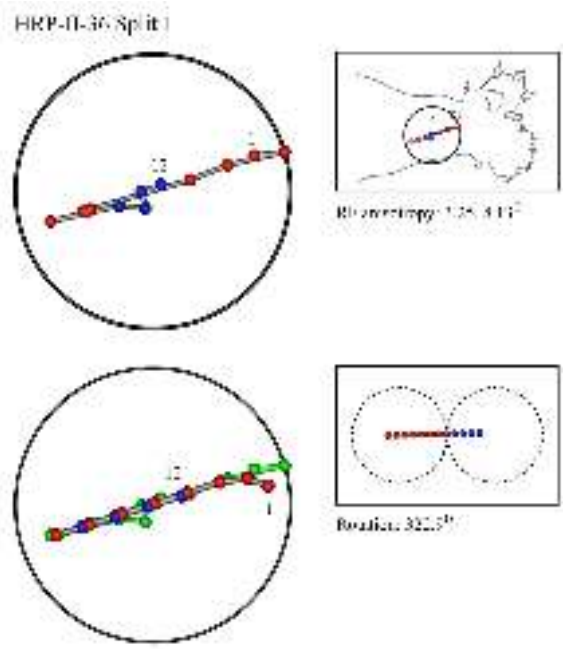

Figure 5c. A “horizontal” penetration in a cat.

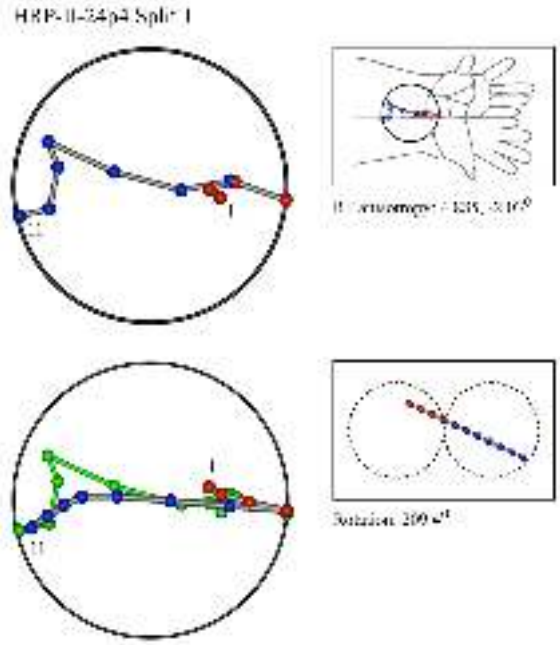

Figure 5d. A “horizontal” penetration in a monkey.

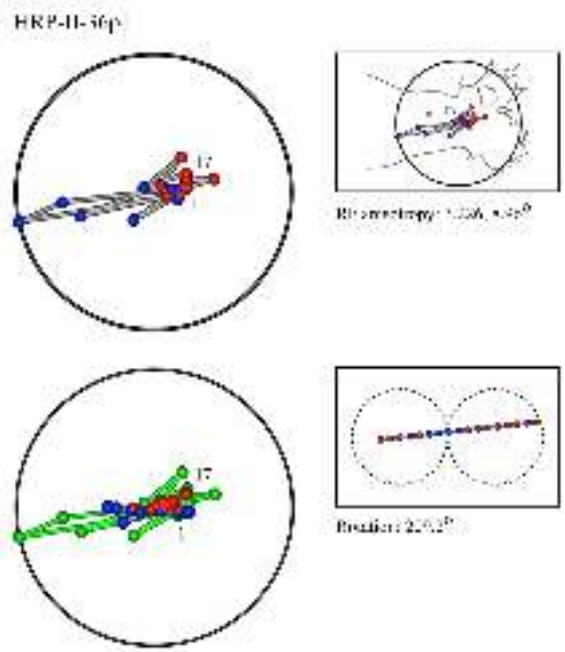

Figure 5e. An "oblique" penetration in a cat.

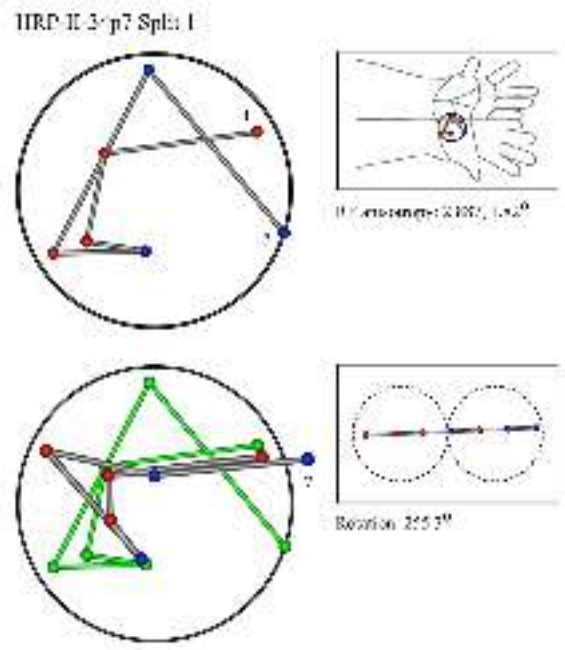

Figure 5f. An "oblique" penetration in a monkey.

Over all datasets, including those provided as supplementary material, the following trends were apparent.

- In 10/22 datasets a type I model fit was found and in 12/22 a type II.
- In 9/22 datasets, a pattern of RFs similar to the "vertical' outcome exemplified in Figure 3a was found, all with a type I fit best-fit configuration. In 8 of these, the RFs were located in the distal limb.

- In 6/22 datasets, a pattern of RFs similar to the "horizontal" outcome exemplified in Figure 3b was found, all with a type II best-fit configuration. In 5 of these the RFs were located in the proximal limb.

- In 7/22 datasets, a pattern of RFs similar to the "oblique" outcome exemplified in Figure 3c was found, 5 of which were of type II, and one of type I. All were in the proximal or middle dispositions on the limb, except for the type I instance, which was proximally located.

- Where sequentially discovered RFs in a single electrode penetration were "split" so as to be able to be fitted to the two-macrocolumn theoretical model, then in 4/6 cases, an initial type II fit was found in the first "split" followed by a type II fit to the second split, and in 2/6 a type II fit was followed by a type I fit - consistent with continued horizontal straight-line passage of the electrode, relative to the size of the cortical representation.

- Best-fit noise/signal ratios tended to increase proximally to distally in expectation with the effects of cortical anisotropy, and the mean RMS noise/signal of 0.62, given the effective electrode sampling radius of <50 μm, implies mean horizontal drift of the recording electrode per dataset, in passage through some or all of the cortical depth, was approximately 80 μm. This appears close to actual electrode drift.

Comparison of Mobius ordering with nested RFs

Nested RFs were obtained for all 22 datasets, and also for all 16 complete full-cortical thickness sequential recordings, so that nests in the "splits" were considered both combined and separately.

In one dataset we found 4 nests, in one 3 nests, in four 2 nests, and only 1 nest in all others. The datasets that had been divided into "splits" for model fitting in all cases but one had only a single nest, and in one case was composed of 3 nests, 2 in one split, and 1 in the other.

There was no one-to-one correspondence between nested RFs and Mobius model constructions. However, where multiple nests were found in a dataset, the RF centroids of the set were relatively distally located on the limb – the first and largest nest more proximally, and the smaller nests more distally on the cat's paw, or on individual fingers of the monkey. In the proximal forearm of both species, large single nests predominated. The proximal/distal differentiation into fewer and more nests corresponded to the proximal/distal trend of type II versus type I model fits.

Figures 6 a and b show two cases at these extremes.

Figure 6a shows the entire overlapping RF set, and the four nests obtained from this dataset. Two of the four nests are each contained within the largest nest, and one nest falls outside all the others. Comparison with Figure 5a, which is the same dataset, shows the modeling result was Type I, vertical - that is, the electrode appears to have passed down through one hypothetical macrocolumn, penetrating first the "clockwise" and top skein of connections, and then the "anticlockwise", bottom skein, as shown by the red and blue dots respectively. It can be seen that the nest that overlapped with no other nest, corresponds to the anticlockwise, bottom, skein.

Figure 6b shows a result from the forearm that is all one nest. The Mobius model had to be fitted in two "splits" implying the dataset was obtained from penetration of three macrocolumns.

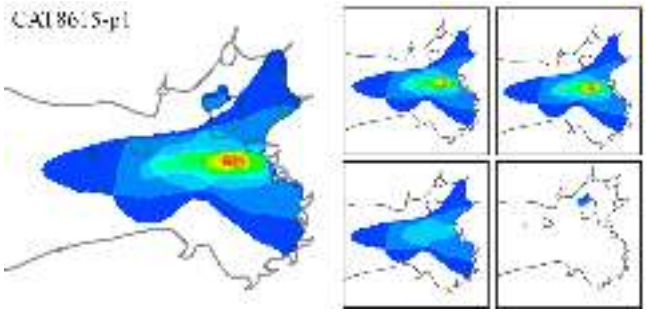

Figure 6a. Nested RFs in the distal paw. (Type I -single macrocolumn) Left: superposition of all RFs in a dataset. Colour spectrum represents density of overlap of RFs; red most dense. Right:. Separate RF nests. Retaining the same colour coding in the complete dataset, these are arranged in order of the number of RFs in each nest – 15, 14, 4 and 3, respectively.

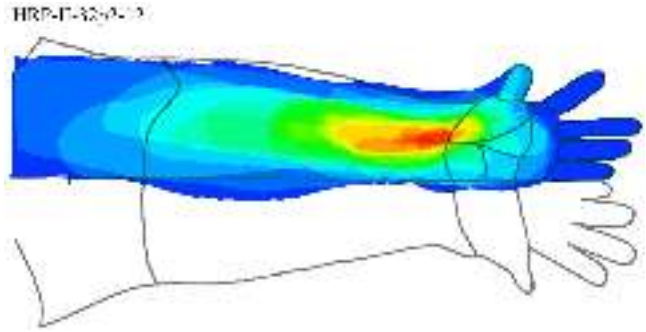

Figure 6b. RF nest in the forearm. (Types II – three macrocolumns). All RFs surround a single centroid.

Conclusions

As originally recognized by Favorov and colleagues, the RFs do not conform to an homotypic map, nor are they wholly random, nor a mixture of homotypic map with uniformly distributed spatial noise. Other than the present model, we know of no other candidate geometry that could explain these results. The expected variant patterns with path of descent of the recording electrode were all encountered in roughly equal numbers, average noise/signal ratios conformed to expectation for spatial noise of recordings, other expectations arising from the effects of position on the limb, and cortical anisotropy were consistently obtained, including consistent modeling of recording sequences that were split for analysis.

Since the theoretical model requires optimization of several parameters, and normalization of scale, rotation and translation, it might be objected that the model could fit any dataset whatsoever. However, the results cannot be dismissed on those grounds, because higher residual values in goodness-of-fit were found if red and blue matching of theoretical and experimental points was other than in accord with the appropriate theoretical oppositely directed lines and clusters of RF centroids.

We propose that the Mobius structure reflects the antenatal organization of synaptic connections, and the RF nests reveal the development, post-natally, of learned functional connections superimposed over the antenatal connection system, in the manner of a palimpsest. Since neurons receiving inputs from an RF nest all receive spatially correlated inputs, neurons in different nests have partially correlated inputs if the nests overlap, while those neurons each at the common center of nests each have unique inputs distinguishing them each from the others. Neurons receiving inputs from non-overlapping nests have no common input. That is, non-overlapping nests represent cells responding to principal components of input spatial cross-correlation, and the RF shapes represent the spatial response tuning of the cortical neurons - analogous to the frequency-domain spatial and temporal

tuning seen in V1 neurons, reported by Issa et al.

The applicability of the Mobius model to both V1 (where anatomical macrocolumns are apparent) and S1 (where they are not) supports the notion that the principle of organization may be general throughout the cortex. All sensory data reach the cortex as some form of primary spatial map, regardless of how the sensory material may be transformed in space, time, or frequency on the sensory pathway, and consequently might be similarly organized for all modalities. We have also argued previously (Wright and Bourke 2013) that similar principles may enable mutual self-organization of synapses and interactions between cortical areas

Continued successful application of this model would enable reformulation of the column concept, not as an anatomical entity dependent on the positions of cell bodies and the overall deployment of axons, but as a functional entity, constructed from the patterning of synaptic connections, whether or not the cells composing the system are separated into obvious columns, or intertwined more completely. This places emphasis much more strongly on horizontal connections (Boucsein et al 2013) and moves away from Mountcastle's minicolumn as a structural entity. The minicolumn, in this view, is the necessary result of order in the horizontal connections, and in this revised concept, the minicolumn does not retain response identity throughout surface to depth of the cortex.

Further experimental testing of the model appears practicable. Indirect testing, similar to the present work, using multiple or single unit analyses, and electrode trajectories exploring small cortical areas, seeking to determine positions of sudden "jumps" - the breaches of continuity, or reversal of RF centroids, that are the crucial model signature. These are likely to be found most clearly with electrode trajectories very close to vertical, and nearly horizontal. Primary sensory cortices of all modalities might be thus explored and other cortical areas for which the sources of inputs can be defined. More accurate quantitative modeling would need to take into account the local distributions of local cell axonal lengths, and the spatial resolution in inputs, relating these to the relative clarity of definition of anatomical columnar definition. Direct testing would place high demands on the capacity of existing techniques to model detailed synaptic connections by the thousands, seeking the underlying Mobius organization. The task is made even more difficult where primary embryonic order is overwritten during subsequent learning. The very large-scale analysis of detailed synaptic connectivity intended in the Human Brain Project and related proposals (Kandel et al 2013) might definitively confirm or refute the model.

Theoretical development of the model may exploit the long-sought advantages of decomposition of the cortex into modular information processing units, and has attractive fundamental properties. It explains how neural connections, self-organised into ultra-small-world configuration, may approach a maximum for speed and energy-efficiency, and indicates how spatio-temporal order may underpin the organisation of signal traffic and learning, since local maps within each macrocolumn have inputs organised in accord with distance and delay from central points, of which the OP singularity is archetypal. The principle of synaptic resource competition, upon which the model is based, also suggests a form of synaptic metabolic entanglement, permitting signal processing complexity, and synaptic information storage, to approach theoretical maxima.

Acknowledgements

A special debt of gratitude is owed to Adrienne Edith Wright.
This work was supported by the Frank P. Hixon Fund of the California Institute of Technology and the Oakley Foundation of New Zealand, and by iVEC, through the use of advanced computing resources located at the University of Western Australia.
The authors are also indebted to Betsy Houston for technical support.

References

Basole, A., White, L. E., and Fitzpatrick, D. (2003). Mapping of multiple features in the population response of visual cortex. *Nature.* 423, 986-990. doi:10.1038/nature01721.

Blakemore, C., and Cooper, G.F. (1970). Development of brain depends on the visual environment. *Nature*. 228, 477-478. doi:10.1038/228477a0.

Blakemore, C., Van Sluyters, R.C. (1975). Innate and environmental factors in the development of the kitten's visual cortex. *J. Physiol.* **248**:3.

Bosking, W.H., Zhang, Y., Schofield, B., Fitzpatrick, D. (1997). Orientation selectivity and the arrangement of horizontal connections in tree shrew striate cortex. *J. Neurosci*. **17**:6.

Boucsein, C., Nawrot, M.P., Schnepel, P., Aertsen, A. (2011). Beyond the cortical column: abundance and physiology of horizontal connections imply a strong role for inputs from the surround. *Front. Neurosci.* **5**:32. doi: 10.3389/fnins.2011.00032.

Braitenberg, V., and Schüz, A. (1991). *Anatomy of the Cortex: Statistics and Geometry.* Berlin, New York: Springer.

Cohen, R., and Havlin, S. (2003). Scale- free networks are ultra-small. *Phys. Rev. Lett.* 90, 058701. doi: 10.1103/PhysRevLett.90.058701.

Da Costa, N.M., Martin, K.A.C. (2010). Whose cortical column would that be? *Front. Neuroanat*. **4**:16 doi: 10.3389/fnana.2010.00016.

DeFelipe, J., Markram, H., Rockland, K. S. (2012). The neocortical column. *Front. Neuroanat*. **6**:22.

Downes, J.H., Hammond, M.W., Xydas, D., Spencer, M., Becerra, V.M., Warwick, K., et al. (2012). Emergence of a small-world functional network in cultured neurons. *PLoS Comput. Biol*. **8**:5 e1002522. doi:10.1371/journal.pcbi.1002522.

Favorov, O., and Whitsel, B.L. (1988a). Spatial organization of the peripheral input to area 1 cell columns: I. The detection of "segregates." *Brain Res. Rev.* 13:25-42.

Favorov, O., and Whitsel, B.L. (1988b). Spatial organization of the peripheral input to area 1 cell columns: II. The forelimb representation achieved by a mosaic of segregates. *Brain Res. Rev.* 13:43-56.

Favorov, O.V., Diamond, M.E. (1990). Demonstration of discrete place-defined columns – segregates - in the cat S1. *J. Comparative Neurol*. **298**:1. doi: 10.1002/cne.902980108.

Favorov, O.V., Diamond, M.E., Whitsel, B.L. (1987) Evidence for a mosaic representation of the body surface in area 3b of the somatic cortex of cat. *Proc. Natl. Acad. Sci. USA* 84:6606-6610.

Gilbert, C.D., Wiesel, T.N. (1989). Columnar specificity of intrinsic horizontal and corticocortical connections in cat visual cortex. *J. Neurosci.* **9**:7.

Girman, S.V., Sauve, Y., Lund, R. D. (1999). Receptive field properties of single neurons in rat primary visual cortex. *J. Neurophysiol*. 82.

Heck, N., Golbs, A., Riedemann, T., Sun, J.J., Lessmann, V., Luhmann, H.J. (2008). Activity dependent regulation of neuronal apoptosis in neonatal mouse cerebral cortex. *Cereb. Cortex.* **18**:6. doi: 10.1093/cercor/bhm165.

Horton, C.H., Adams, D.L. (2005). The cortical column: a structure without a function. *Philos. Trans. R. Soc. Lond. B Biol. Sci.* 360. doi: 10.1098/rstb.2005.1623.

Hubel, D.H. (1981). Acceptance Address. The Nobel Prize in Medicine.

Hubel, D.H., Wiesel, T.N. (1959). Receptive fields of single neurones in the cat's striate cortex. *J. Physiol*. 148.

Issa, N.P., Rosenberg, A., Husson, T.R. (2008). Models and measurements of functional maps in V1. *J. Neurophysiol*. 99. doi: 10.1152/jn.90211.2008.

Kaas, J.H., Nelson, R.J., Sur, M., Lin, C.S., and Merzenich, M.M. (1979). Multiple representations of the body within the primary somatosensory cortex of primates. *Science*. 204, 521-523. doi: 10.1126/science.107591.

Kandel, E.R., Markram, H., Matthews, P.M., Yuste, R., and Koch, C. (2013). Neuroscience thinks big (and collaboratively). *Nature Neuroscience.* 14, 659 - 664. doi:10.1038/nrn3578.

Kaschube, M., Schnabel, M., Löwel, S., Coppola, D.M., White, L.E., and Wolf, F. (2010). Universality in the evolution of orientation columns in the visual cortex. *Science*. 330, 1113 - 1116. doi: 10.1126/science.1194869.

Keil, W., Kaschube, M., Schnabel, M., Kisvarday, Z.F., Löwel, S., and Coppola, D.M., et al. (2012). Response to comment on "Universality in the evolution of orientation columns in the visual cortex". *Science*. 336, 413. doi: 10.1126/science.1206416.

Marshall, W.H., Woolsey, C.N., Bard,P. (1941). Observations on cortical somatic sensory mechanisms of cat and monkey. *J. Neurophysiol.* 4.

Mountcastle, V.B., Berman, A.L., Davies, P.W. (1955). Topographic organization and modality representation in first somatic area of cat's cerebral cortex by method of single unit analysis. *Am. J. Physiol.* 183.

Mountcastle, V.B. (1997). The columnar organization of the neocortex. *Brain*. 120, 701-722.

Muir, D.R., Da Costa, N.M.A., Girardin, C.C., Naaman, S., Omer, D. B., Ruesch, E., et al. (2011). Embedding of cortical representations by the superficial patch system. *Cereb. Cortex.* **21**:10. doi: 10.1093/cercor/bhq290.

Obermayer, K., Blasdel, G.G. (1993). Geometry of orientation and ocular dominance columns in monkey striate cortex. *J. Neurosci.* **13**:10.

Paik, S.B., and Ringach, D.L. (2011). Retinal origin of orientation maps in visual cortex. *Nat. Neurosci*. 14, 919 – 926. doi:10.1038/nn.2824.

Purves, D., Riddle, D.R., La Mantia, A-S. (1992) Iterated patterns of brain circuitry (or how the cortex gets its spots). *TINS*. 15, 362-368.

Rakic, P. (1988). Specification of cerebral cortical areas. *Science*. 241, 170-176. doi: 10.1126/science.3291116.

Rakic, P. (2008). Confusing cortical columns. *PNAS*. 105, 12099-12100.

Rakic, P. (2009). Evolution of the neocortex: Perspective from developmental biology. *Nature Review Neurosci*. 10, 724-735. doi:10.1038/nrn2719.

Sharma, J., Angelucci, A., Rao, S.C., Sur, M. (1995). *Relationship of Intrinsic Connections to Orientation Maps in Ferret Primary Visual Cortex: Iso-orientation Domains and Singularities.* San Diego, CA: Presented at Society for Neuroscience.

Swindale, N.V. (1996). The development of topography in the visual cortex: a review of models. *Network 7*, 161-247.

Woolsey, T.A., and Van der Loos, H. (1970). The structural organization of layer IV in the somatosensory region (S1) of mouse cerebral cortex: the description of a cortical field composed of cytoarchitectonic units. *Brain Res*. 17.

Wright, J.J. (2009). Generation and control of cortical gamma: findings from simulation at two scales. *Neural Netw*. **22**:4.

Wright, J.J. (2010). Attractor dynamics and thermodynamic analogies in the cerebral cortex: synchronous oscillation, the background EEG, and the regulation of attention. *Bull. Math. Biol*. 73. doi: 10.1007/s11538-010-9562-z.

Wright, J.J., Bourke, P.D. (2013). On the dynamics of cortical development: synchrony and synaptic self-organization. *Frontiers in Computational Neuroscience*. doi: 10.3389/fncom.2013.00004.